




Research Article

Future search algorithm for optimal integration of distributed generation and electric vehicle fleets in radial distribution networks considering techno-environmental aspects



Varaprasad Janamala¹  · U. Kamal Kumar² · Thandava Krishna Sai Pandraju³

Received: 14 July 2020 / Accepted: 4 March 2021 / Published online: 17 March 2021

© The Author(s) 2021 

Abstract

In this paper, a new nature-inspired meta-heuristic algorithm called future search algorithm (FSA) is proposed for the first time to solve the simultaneous optimal allocation of distribution generation (DG) and electric vehicle (EV) fleets considering techno-environmental aspects in the operation and control of radial distribution networks (RDN). By imitating the human behavior in getting fruitful life, the FSA starts arbitrary search, discovers neighborhood best people in different nations and looks at worldwide best individuals to arrive at an ideal solution. A techno-environmental multi-objective function is formulated using real power loss, voltage stability index. The active and reactive power compensation limits and different operational constraints of RDN are considered while minimizing the proposed objective function. Post optimization, the impact of DGs on conventional energy sources is analyzed by evaluating their greenhouse gas emission. The effectiveness of the proposed methodology is presented using different case studies on Indian practical 106-bus agriculture feeder for DGs and 36-bus rural residential feeder for simultaneous allocation of DGs and EV fleets. Also, the superiority of FSA in terms of global optima, convergence characteristics is compared with various other recent heuristic algorithms.

Keywords Electric distribution networks · Loss minimization · Voltage stability enhancement · Distributed generation · Electric vehicle fleet · Greenhouse gas emission minimization

1 Introduction

The exhausting fuel sources for conventional energy sources (CES), non-expanding transmission and distribution networks and ever increasing demand for electricity have made the power system operation and control very complex. On the other side, the dependency on CES is considerably high for energy balance and causing for greenhouse gases (GHG) emission and consequently contributing for environment pollution significantly. Under these circumstances, integration of renewable energy

sources (RES) and adoption of electric vehicle (EV) technology have become mandatory in various power grids and transportation sectors across the world respectively [1]. As per International Renewable Energy Agency (IRENA) statistics released in March 2019, the total RE integration in 2018 has been reached to 2364.4 GW including off-grid across the world [2]. In 2018, the global electric car fleet exceeded 5.1 million and the growth is almost double as compared with 2017 statistics [3]. From these statistics, it can be said that these two exponential trends are getting high attention across the world due to their potential for

✉ Varaprasad Janamala, varaprasad.janamala@christuniversity.in | ¹Department of Electrical and Electronics Engineering, Faculty of Engineering, Christ (Deemed To Be University), Bangalore, Karnataka 560 074, India. ²Department of Electrical and Electronics Engineering, Sree Vidyanikethan Engineering College, Tirupati, Andhra Pradesh 517 102, India. ³Department of Electrical and Electronics Engineering, Dhanekula Institute of Engineering and Technology, Vijayawada, Andhra Pradesh 521 139, India.



reducing GHG emission and contributing towards sustainable practices. However, the intermittent nature of RES and unpredictable nature of EV load pattern needs to be addressed potentially for avoiding the possible operational and controlling issues in power systems. By integrating RES and EV charging stations (CSs)/parking lots (PLs)/ fleets at improper locations, the expected technical benefits to the power system can become negative. In this era, performance analysis of RDNs w.r.t. different type of loads such as residential, industrial, commercial, agriculture and electric vehicle etc., is inevitable and preventive measures for ensuring high reliable supply are needed to focus much.

As known, the major weak segment in power systems is the distribution system and optimization of its performance is always an important criterion in power system operation and control. Optimal network reconfiguration (ONR), installation of capacitor banks (CBs), and integration of distribution generation (DGs) are some of the remedial ways for some extent to improve the performance of radial distribution networks (RDN). The major objective of optimal allocation of DGs problem is to improve the performance of the distribution system and maximization of economic benefits to the utilities. In literature, optimal allocation of DGs has been addressed highly by various traditional (non-heuristic) and non-traditional (heuristic) approaches, whereas optimal allocation of EV infrastructure or charging stations (CSs) is also getting high attention among the researchers in recent times. Over the past few decades, numerous methodologies have been proposed by different researchers for allocating the DGs in distribution system optimally [4, 5]. Although the optimal allocation of DGs problem in RDNs is widely addressed in literature, sufficient research is not focused considering emerging electric vehicle load penetration. In order to provide charging infrastructure, optimal allocation of EV fleets is an important factor since there is a possibility for degrading the performance of RDNs due to their integration at inappropriate locations. The methodologies can be classified like non-heuristic approaches (NHA) and heuristic approaches (HA). In comparison, HAs are simpler, derivative-free and easy to implement for solving the complex, non-linear optimization problems than NHAs and hence some of the recent HAs applied for solving the DGs allocation problem have been discussed here.

In [6], chaotic stochastic fractal search (CSFS) algorithm is applied to solve DG allocation for real power loss minimization. In [7], spring search algorithm (SSA1) and in [8], gbest-guided artificial bee colony (GABC) algorithm are proposed for solving the simultaneous allocation of DGs and CBs by aiming techno-economic-environment benefits in network operation. In [9], considering real power loss minimizations the DGs are integrated optimally using

teaching–learning based optimization (TLBO) algorithm. In [10], bacterial foraging optimization algorithm (BFOA) is proposed for simultaneous allocation of DGs and CBs towards loss minimization and voltage profile improvement. Hybrid grey wolf optimizer (HGWO) is proposed for loss minimization via optimal allocation of multi-type DGs in 33-, 69- and Indian 85-bus systems [11]. In [12], multi-type DGs and CBs are optimized using optimal power flow (OPF) embedded with generic analytical expressions for determining the sizes. In [13], an enhanced genetic algorithm (EGA) is proposed for minimizing the real power losses via allocating simultaneous DGs and CBs in the network. In [14], war optimization algorithm (WOA), particle swarm optimization (PSO), cuckoo search algorithm (CSA), firefly algorithm (FA) and bat algorithm (BA) are applied for sizing the multiple solar PV systems towards loss minimization. In [15], weight improved particle swarm optimization algorithm (WIPSO) and self adaptive differential evolution algorithm (SADE) have been proposed for solving the simultaneous allocation of renewable type DGs and CBs by minimizing the multi-objective function formed using real and reactive power losses and voltage profile. In [16], ant lion optimization (ALO) algorithm is proposed for minimizing the multi-objective function using real power loss, voltage profile and voltage stability via optimally locating and sizing the renewable DGs. In [17], grasshopper optimization algorithm (GOA) is adopted for allocating multiple DGs, fixed and switched CBs for minimizing real power losses. In [18], PSO is adopted for sizing the multiple DGs and CBs for minimizing the economic aspects at network operation and planning stages. In [19], a shuffled frog leaping algorithm (SFLA) is applied for minimizing real power loss and consequently economic efficiency of distribution system operation is evaluated via allocating the multiple DGs. In [20], a multi-objective whale optimization algorithm (MOWOA) is applied for identifying the locations and sizes of solar PV and wind turbine systems considering different types of load models. The objective function is formulated for optimizing the real power loss index, voltage index and cost benefit indices simultaneously. Salp swarm algorithm (SSA2) [21] and water cycle algorithm (WCA) [22] are proposed for attaining techno-economic-environmental benefits via simultaneous allocation of DGs and CBs. In [23], hybrid approach using grasshopper optimization algorithm (GOA) and cuckoo search algorithm (CSA) is proposed for allocating the multi-type multiple DGs towards technical benefits. In [24], hybrid approach using fuzzy logic controller (FLC), ALO and PSO is proposed for solving the renewable type DG integration problem towards technical benefits. In [25], elephant herding optimization (EHO) algorithm is applied for determining single multi-type DG location and size considering techno-economic aspects. In [26], ALO is proposed for optimal sizing

of DGs considering techno-economic benefits. In [27], a multi-objective PSO (MOPSO) is applied for solving optimal allocation of renewable DGs and CBs.

Recently, the optimal allocation of DGs problem is addressed using quasi-oppositional chaotic symbiotic organisms search (QOCSOS) algorithm by aiming for reduction in real power loss, improvement in voltage profile and enhancement in voltage stability [28, 29]. The study revealed that the DGs with non-unity power factor can improve RDNs performance significantly than the DGs with unity power factor. Coyote optimization algorithm (COA) [30] is proposed for optimal integration of DGs in RDNs considering multi-objective function, formed using real power loss, operating cost and voltage stability. In [31], an improved variant of COA as enhanced coyote optimization algorithm (ECOA) is proposed for solving simultaneous optimal network reconfiguration and DG allocation problem. In [32], harmony search algorithm (HSA) is pursued for solving simultaneous optimal network reconfiguration and DG allocation problem in unbalanced RDNs. In [33], chaotic sine cosine algorithm (CCSCA) and in [34], an improved raven roosting optimization (IRRO) algorithm are introduced for solving multi-objective optimal allocation of multiple DGs problem. In similar to [35], a new pathfinder algorithm (PFA) is proposed for obtaining simultaneous optimal network reconfiguration and DG allocation. Similarly, hybrid genetic particle swarm optimization (HGPSO) [36], stochastic fractal search optimization algorithm (SFSOA) [37] and biogeography-based optimization (BBO) [38] are some of such recent meta-heuristic approaches for solving optimal allocation of DGs problem considering technical aspects. Further, the reader can also find recent reviews on distribution system performance improvement via optimal allocation of DGs, CBs and network reconfiguration and their combination [39–42]. At this stage, it can be concluded that the performance of RDNs can be improved significantly via optimal allocation of DGs and/or ONR problem.

On the other side, optimal allocation of EV charging infrastructure has been motivated and attracted by various researchers in recent times. According to the survey presented in [43], optimal allocation of EV charging infrastructure problem has been solved in three categories, (1) transportation-network, (2) distribution-network and (3) transportation-distribution-networks. Considering the possibility of degradation in the performance of RDNs due to EV fleet load, integration of EV charging stations at optimal location is essential. In line to the DGs allocation methods referred above, distribution-network based optimal allocation of EV fleets along with DGs allocation is proposed in this paper and claimed as one of the major contributions in this paper. Notably, the optimal allocation of DGs problem is a non-linear multi-objective

optimization problem which needs to be solved for discrete and continuous variables simultaneously. In addition, the problem can become more complex for simultaneous allocation of DGs and EV fleets in large-scale RDNs and needs large computational time. According to the no-free-lunch theorem [44], there is no single specific heuristic algorithm which can solve all type of optimization problems. Hence, the researchers are still inspiring to introduce new heuristic algorithms and applying them to different optimization problems.

In the above reviewed literature, there are many such heuristic and meta-heuristic algorithms that have been used for solving optimal allocation problem. To the best of authors' knowledge, future search algorithm (FSA) [45] has not been applied for solving the either optimal allocation of DGs problem and/or optimal allocation of EV fleet problem in RDN. In addition, most of the works have been analyzed considering multi-objective function for techno-economic aspects, but limited numbers of works have been only focused on techno-environmental aspects in the DG allocation problem [7, 21, 22]. Also, the charging infrastructure required for serving the emerging EV load demand is not focused much. In competition to the existing literature works, FSA is first applied for solving only DGs allocation problem alone and later simultaneous allocation of DGs and EV fleets is proposed as a countermeasure to the degrading performance of RDN w.r.t. EV fleet allocation.

Rest of the paper is organized as follows: Sect. 2 addressed the modeling of DGs and EV fleet load. In Sect. 3, a multi-objective optimization problem constrained by various technical, operational and planning issues is presented. In Sect. 4, the mathematical relations of FSA and the steps used in solving the formulated multi-objective problem is explained. In Sect. 5, various case studies on practical agriculture and rural residential feeders are presented. The major contributions, research findings and the superiority of proposed FSA approach over existing algorithms is concluded in Sect. 6.

2 Modeling of relevant concepts

In this section, static modeling of DGs and EV fleet load are explained considering RDN load flow study.

2.1 Distribution generation

The electric power generation sources in different forms placed near to the load centres and integrated directly to the distribution networks are known as DGs. As per the active and/or reactive power compensation, these DGs

can be modeled as negative loads and their classification along with modeling as follows:

2.1.1 Type-1 DG (active power compensation sources)

Photovoltaic, micro turbines and fuel cells which are incorporated into the main grid with the help of converters/inverters are good examples of real power compensation sources. In this model, the real power load at bus-*i* will be reduced by an amount equal to DG’s real power output with unity power factor (upf) and is given by:

$$P_{di,new} = P_{di,base} - P_{DG,i} \tag{1}$$

2.1.2 Type-2 DG (reactive power compensation sources)

Shunt CBs (in either fixed or/and switched form) are the best examples for reactive power compensation sources particularly at the distribution network. In this model, the reactive power load at bus-*i* will be reduced by an amount equal to DG reactive power output and is given by:

$$Q_{di,new} = Q_{di,base} - Q_{DG,i} \tag{2}$$

2.1.3 Type-3 DG (complex power compensation sources)

Wind farms and synchronous generators are example of complex power compensation sources. The power factor lies between 0.7 and 1. In this model, the active power will be reduced by an amount equal to DG active power and reactive power will be either increment/decrement by an amount equal to DG reactive power load at bus-*i* and is given by:

$$P_{di,new} + jQ_{di,new} = (P_{di,base} - P_{DG,i}) + j(Q_{di,base} \pm P_{DG,i} \tan(\phi_{DG,i})) \tag{3}$$

where $P_{di,base}$ and $Q_{di,base}$ are the active and reactive power loads at bus-*i*, respectively; $P_{di,new}$ and $Q_{di,new}$ are the modified active and reactive power loads with DG integration at bus-*i*, respectively; $P_{DG,i}$ and $Q_{DG,i}$ are the active and reactive power generations/injections by DG integrated at bus-*i*, respectively; $\phi_{DG,i}$ is the power factor angle of DG at bus-*i*.

As per the above models, the DGs compensate either active power or reactive power or both and cause a decreased net loading effect on the feeder. The decreased load balances usually at slack bus in load flow studies. By the redistribution of power flows with reduced loading, the net voltage profile, transmission loss and stability margins can improve significantly.

2.2 Electric vehicle fleet

Here, it is assumed here that all types of EVs in an EV fleet are integrated to the utility via AC/DC converter with an operating power factor of nearly unity. It is also assumed that the total number EVs in an EV fleet are arranged in *p* rows and *q* columns and each EV may have different power ratings [46]. Since EV is basically powered by batteries, its corresponding loading effect during charging mode is modeled by considering voltage dependent load modeling [47]. By summing all EV power ratings, the total real power demand of an EV fleet is determined. The following Eqs. (4) and (5) represents the real and reactive power demand at bus-*n* after EV fleet integration respectively.

$$P_{d(n)}^t = P_{L(n)}^0 \times \left(\frac{V_{L(n)}^t}{V_{L(n)}^0}\right)^\alpha + \sum_{i=1}^p \sum_{j=1}^q \left[P_{ev,ij} \times \left(\frac{V_{L(n)}^t}{V_{L(n)}^0}\right)^{\alpha_{ev}} \right] \tag{4}$$

$$Q_{d(n)}^t = Q_{L(n)}^0 \times \left(\frac{V_{L(n)}^t}{V_{L(n)}^0}\right)^\beta + \sum_{i=1}^p \sum_{j=1}^q \left[Q_{ev,ij} \times \left(\frac{V_{L(n)}^t}{V_{L(n)}^0}\right)^{\beta_{ev}} \right] \tag{5}$$

$$Q_{ev,ij} = P_{ev,ij} \times \tan(\phi_{ev,ij}) \tag{6}$$

where $P_{L(n)}^0$ and $Q_{L(n)}^0$ are nominal real and reactive power loads at bus-*n* respectively; $P_{L(n)}^t$ and $Q_{L(n)}^t$ are modified real and reactive powers at time *t* respectively; $P_{d(n)}^t$ and $Q_{d(n)}^t$ are the real and reactive power loads at location *n* after integration of EV load respectively; $P_{ev,ij}$ and $Q_{ev,ij}$ are the real and reactive loads due to an EV at *i*th row and *j*th column in the fleet; $V_{L(n)}^0$ and $V_{L(n)}^t$ are the voltage magnitude of bus-*n* at nominal and time specified respectively; α and β are the exponents for real and reactive powers respectively; α_{ev} and β_{ev} are the exponents of EV’s real and reactive power loads respectively.

3 Problem formulation

In the operation and control of RDN, minimization of real power loss is one of the major goals. This can be achieved mainly by improving the voltage profile across the network, and consequently loss can reduce by having reduced current flow through each branch/element. In addition, an improved voltage profile can result in enhanced voltage stability.

Primarily, the voltage magnitude at any bus-*j* (V_j) in the distribution system is dependent on its active power load (P_j), reactance of the branch (x_{ij}), power factor (*pf*) or in

other words, reactive power load (Q_j), and preceding end bus voltage (V_j) as in:

$$V_j = \left(V_i - \frac{Q_j X_{ij}}{V_i} \right) - j \frac{P_j X_{ij}}{V_i} \tag{7}$$

Hence, by controlling active power and reactive power demands with different types DGs, the voltage deviation *w.r.t.* reference voltage (V_i) has to be minimized for having adequate voltage profile and stability margins and consequently reduced real power losses in the network can be achieved significantly.

3.1 Objective function

In order to achieve efficient operation, minimization of active power loss is one of important aspects and is determined using (8):

$$\min f_1 = \min \left\{ P_{loss} = \sum_{k=1}^{nbr} \frac{r_k (P_j^2 + Q_j^2)}{V_i^2} \right\} \tag{8}$$

where nbr is the number of branches in the network, r_k is the resistance of branch- k , P_{loss} the total active power loss in the network.

By various power system blackout incidents across the world, voltage stability has become one of the primary concerns of the system operator [48]. Hence by optimizing the penetration level of different types of DGs and EV fleet, the network voltage stability is aimed to maximize. Perhaps, voltage stability assessment of RDN and its enhancement are the typical tasks to the system operator. In this paper, the impact of DGs and EV fleet on voltage stability of distribution network is analyzed using the methodology proposed in [49] and given by (9).

$$VSI_i = |V_i|^4 - 4(P_{di} X_{ij} + Q_{di} r_{ij}) \geq 0 \tag{9}$$

where VSI_i = voltage stability index of node- i ($i = 2, 3, \dots, nbus$); r_{ij} and x_{ij} are the resistance and reactance of the branch connected between bus- i and bus- j respectively; P_{di} and Q_{di} are the real and reactive power loads at bus- i respectively; $|V_i|$ is the voltage magnitude of bus- i . The condition for stable operation of the radial distribution network is $VSI_i \geq 0$. The bus with lowest VSI can be treated as a critical bus for voltage collapse and its corresponding index value can be considered as a stability index for the entire network.

After assessing system stability, the major focus of this paper is to enhance it by means of allocating DGs and EV fleets optimally. Hence maximization of the lowest VSI_i of the entire network can ensure increased stability margin.

$$\min f_2 = \min \{ 1 / \min (VSI_{i \in nbus}) \} \tag{10}$$

Finally, the overall multi-objective function is formulated using real power loss and voltage stability index, as given in Eq. (11).

$$OF = \min (f_1 + f_2) \tag{11}$$

In Greenhouse Gas (GHG) emission, CO_2 , SO_2 and NO_x are the most effective pollutants with power generating stations. By reducing the real power loss and dependency on grid power via optimal allocation of DGs and EV fleets, the power generation from grid reduces and consequently environmental benefits can be achieved. The emission factors with grid power are $NO_x = 5.06$ lb/MWh, $SO_2 = 11.6$ lb/MWh and $CO_2 = 2031$ lb/MWh [50]. Mathematically, the emission can be calculated as follows:

$$E_{Grid} = (CO_2 + NO_x + SO_2) \times (P_D + P_{loss}) \tag{12}$$

By knowing the total power generation includes network real power demand (P_D) and total real power losses (P_{loss}) in distribution, the emission (E_{Grid}) from CES can be determined.

3.2 Operational constraints

The aforementioned objective functions are optimized by having the following VSI, node voltage (V_i) and branch flow ($|S_l|$) operational constraints, real power ($P_{DG,g}$) and reactive power generation ($P_{DG,g}$) generation limits by DGs compensation in the network.

$$VSI_i > 0 \quad i = 1, 2, \dots, nbus \tag{13}$$

$$V_{min} \leq V_i \leq V_{max} \quad i = 1, 2, \dots, nbus \tag{14}$$

$$|S_l| \leq |S_{l,max}| \quad l = 1, 2, \dots, nbr \tag{15}$$

$$P_{DG,g} \leq \sum_{i=1}^{nbus} P_{di} + \sum_{i=1}^{nfl} P_{dfi} \tag{16}$$

$$Q_{DG,g} \leq \sum_{i=1}^{nb} Q_{di} + \sum_{i=1}^{nfl} P_{dfi} \tan(\phi_{fi}) \tag{17}$$

where nfl is the number of EV fleets, P_{df} and ϕ_f are the power rating of one EV fleet and power factor of AC/DC converter respectively; V_{min} and V_{max} are the lower and upper limits for the bus voltage magnitude, respectively; $S_{l,max}$ is the maximum power flow limit of branch- l ; $P_{DG,g}$ is the total real power generation by all DGs in the network,

P_{df} is the total active power demand of the EV fleets in the network.

4 Future search algorithm

All individuals on the planet search for the best life. In the event that any individual discovered that his life isn't acceptable, he attempts to imitate the life of the best individual around the globe. The future search algorithm (FSA) utilizes this conduct to locate the best arrangements [45]. The FSA is defined by numerical conditions. It can refresh the irregular beginning and it uses the nearby inquiry between individuals, what's more, the worldwide pursuit between the narrative's ideal people. The others HSA start its means by a random population and it formulates its iterations dependent on the best optima of the random beginning. This best population might be a long way from the initial population, this makes the HSA take many iterations to come to the global optima. The FSA can defeat this issue and it refreshes the irregular population each every iteration. In every HSA, there is a local best population between the multi-variables and global optima between the iterations. Some of HSA update its new population dependent on the nearby best population as it were. In any case, the others update its new population dependent on the global best optima as it were. These strategies may take a long number of iterations. The FSA uses the local best solution and the global optima for finding the best population. Some of HSA have more and complex mathematical models which can take additional time and a long number of iterations to come to the global optima.

4.1 Modeling of future search algorithm

The proposed FSA is worked by simple mathematical conditions. In this section, the fundamental mathematical equations involved in the FSA are presented.

Generate random initialization using Eq. (18), in which S is the solution, k is the current solution, d is the dimension of search space or number of countries, L_b and U_b are the lower and upper boundaries of the variables in the optimization problem.

$$S(k, :) = L_b + (U_b - L_b) * rand(1, d) \quad (18)$$

The objective function of each initial population is defined as a local solution (LS) and the best among all is defined as a global solution (GS). The FSA uses both LS and GS to find the optimal solution in its process.

The exploitation feature of the FSA is modeled using Eq. (19) by using the best influenced person or LS of each country.

$$S(k, :)_L = (LS(k, :) - S(k, :)) * rand() \quad (19)$$

The next step is to characterize the exploration feature of the FSA which uses the global influenced person or GS and is given in Eq. (20).

$$S(k, :)_G = (GS - S(k, :)) * rand() \quad (20)$$

By observing the local and global influenced persons across the world, each person may change his way of leading the life or current variables and it is modeled as given in Eq. (21) using the local and global influenced solutions.

$$S(k, :) = S(k, :) + S(k, :)_L + S(k, :)_G \quad (21)$$

At this stage, the FSA updates the GS and LS and uses to modify the initial population using Eq. (22) and this is the major characteristic of FSA to define its exploration ability than other HSA.

$$S(k, :) = GS + (GS - LS(k, :)) * rand() \quad (22)$$

This process repeats until the convergence criteria reaches by computing LS and GS using Eq. (19) and Eq. (20) respectively, finding the new solution using Eq. (12) and update LS, GS, and initial population of Eq. (18) using Eq. (22). The population size indicates the number of nations searching by a person for his comfortable life. The more nations mean the more local influenced persons (LSs). These individual local best persons can again be influenced by the global best person (GS). Hence defining new GS and LS at each iteration and again using them for updating the optimal solution within the same iteration is the key feature of FSA for outperformance than the other HSA. Generally, the maximum number of iterations (k_{max}) are taken to stop the iteration process of all HASs and it remains the same in FSA also. This stage can be treated as that the person reaches a satisfactory level in life or his goal, by which he may stop searching further. Also, from the mathematical equations point of view, FSA is also said to be the simplest without necessity to tune any controlling variables and proven its superiority than various other HSAs by its fast convergence rate characteristics and capability to escape premature convergence [45].

4.2 Application of FSA for solving simultaneous optimal allocation of DGs and EV fleets

The solution methodology of FSA for solving optimal allocation of DGs and EV fleet problem is followed the following steps.

Step 1 Read the test system bus data and branch data, dimension of search space d (includes number of DGs,

number of EV Fleets and size of DGs) and number of countries n and maximum number iterations k_{max} .

Step 2 Generate initial population using Eq. (18) and evaluate the objective function value using Eq. (11). Since the locations of DGs and EV Fleets are discrete variables, round(x) function is used and whereas DG sizes remain the same as generated using random number theory within the search space. From the solutions, define each solution as a local solution (LS) and best among all as a global solution (GS).

Step 3 Perform exploitation stage related to each country for each LS using Eq. (19) and exploration stage related to overall world using Eq. (20) respectively.

Step 4 Using LS and GS in Step (2) and Step (3), update the solution of each person using Eq. (21) and update LS and GS solutions.

Step 5 Update the initial random population generated at Step (2) using Eq. (18) for new population using Eq. (22) and check for updating LS and GS before increment in iteration count k .

Step 6 Check for $k = k_{max}$.

Step 7 If not, repeats Step (3) to Step (6), else, stop and print the results.

5 Results and discussion

In this section, the effectiveness of the proposed FSA for solving optimal allocation of CBs/DGs problem is demonstrated. For the purpose, the simulation studies on two real-time test systems namely 106-bus agricultural feeder and 36-bus system represents a small portion of residential feeder in Srikalahasti, Chittoor, AP, are presented and discussed here. The bus data and line data of these test systems are provided in Appendix A1 and A2 respectively. The simulations are performed in a PC with specification of 4 GB, 64-bit OS and Intel® Core™ i5-2410 M CPU @ 2.3 GHz processor using MATLAB program [51].

5.1 Practical 106-bus agriculture feeder

The practical system has 106 buses interconnected by 105 branches and operating at 11 kV. In this system, the following case studies are performed for two scenarios: (1) peak loading condition and (2) average loading conditions.

Case 1: Optimal allocation of CBs.

Case 2: Optimal allocation of DGs operating at unity power factor.

Case 3: Simultaneous allocation of CBs and DGs operating at unity power factor.

5.1.1 Scenario-1: peak loading condition

The peak constant power load of the system is (1218.68 kW + j 775.947 kVAr). According to voltage-dependent load modeling [52], the exponents for real and reactive powers are considered as 0.08 and 1.6 respectively for representing the agriculture loads such as pumps, fans and motors. From the load flow results, it is observed that total system load of (1216.372 kW + j 747.002 kVAr) and the test system is suffering from a total loss of (27.78 kW + j 20.21 kVAr). Also, the lowest voltage magnitude and stability index are observed as 0.9709 p.u. and 0.8887 at 105th bus respectively.

Case 1: In this case, FSA is applied to minimize real power losses via optimally allocation three CBs in the system. Also, the smallest size of CB is chosen as 50 kVAr. Under ideal VAr compensation (i.e., total reactive load on network made zero), the system has a total loss of (19.8591 kW + j 14.4472 kVAr). It means, by optimal allocation of CBs, the objective function value should not be less than 19.8591 kW. The best locations (buses 61, 104 and 106) and sizes in kVAr (i.e., 200, 200, 100) obtained by FSA are given in Table 1. In comparison to the base case, the improved performance of the system is as follows: the losses are decreased to 21.1203 kW from 27.78 kW and the minimum voltage magnitude and VSI at 100th bus are observed as 0.9787 p.u. and 0.9176 respectively.

Table 1 FSA results of real-time 106-bus feeder under peak loading conditions

Case	CBs (kVAr)	DGs (kW)	P_{loss} (kW)	Q_{loss} (kVAr)	V_{min} (p.u.)	VSI
Base	–	–	27.78	20.21	0.9709 (105)	0.8887
1	200 (61) 200 (104) 100 (106)	–	21.1203	15.3647	0.9787 (100)	0.9176
2	–	399 (32) 281 (16) 466 (10)	8.6547	6.2961	0.9885 (105)	0.9546
3	200 (47) 150 (23) 200 (79)	446 (57) 463 (95) 153 (68)	1.988	1.4464	0.996 (44)	0.9840

Case 2: In this case, FSA is applied to maximize voltage stability index via optimally allocation three DGs in the system. Under ideal active power compensation (i.e., total active load on a network made zero), the VSI of the system is 0.964. By integrating DGs with upf, the VSI may not be more than this value. Using FSA, the optimal locations (buses 32, 16 and 10) and DG sizes in kW (i.e., 399, 281 and 466), the VSI is reached to 0.9546. Correspondingly, the system real power loss and minimum voltage magnitude at 105th bus are 8.6547 kW and 0.9885 p.u. respectively.

Case 3: In this case, FSA is applied to optimize multi-objective function of loss plus voltage stability index via optimally simultaneous allocation of three DGs and three CBs in the system. The best objective function value 2.9723 is obtained by FSA via DGs at buses 57, 95, and 68 with sizes in kW, 446, 463 and 153, and CBs at buses 47, 23, and 79 with sizes in kVAr, 200, 150 and 200. The real power losses are The minimum voltage magnitude of 0.996 p.u. is observed at 44th bus and correspondingly VSI is reached to 0.984.

The results of three cases are given in Table 1. The voltage profiles of test system under different conditions are given in Fig. 1. In comparison to the base case, the real power losses of 1.988 kW, which have decreased by 92.8427%.

5.1.2 Scenario-2: average loading condition

On the other side, the system has an average constant power load of (1106.251 kW + j 743.99 kVAr). Considering voltage-dependent load modeling, the load flow is performed and observed as total load (1104.323 kW + j 718.5 kVAr), total loss of (23.517 kW + j 17.108 kVAr), and the lowest voltage magnitude and stability index are observed as 0.9732 p.u. and 0.8972 at 105th bus respectively.

Case-1: The case study is repeated by considering average loading conditions. By having CBs at buses 8, 98 and 77 with a capacity of 150 kVAr, 200 kVAr and 200 kVAr respectively, the losses are decreased to 16.925 kW from 23.517 kW and minimum voltage at 105th bus is increased to 0.9805 p.u. from 0.9732 p.u. and stability index improved to 0.9242 from 0.8972.

Case-2: Similarly, the VSI is optimized considering average loading conditions on the system. The results of FSA are as follows: the optimal locations (buses 97, 7 and 8) and DG sizes in kW (i.e., 373, 220 and 453), the VSI is reached to 0.9653. Correspondingly, the system real power loss and minimum voltage magnitude at 105th bus are 7.6946 kW and 0.9912 p.u. respectively.

Case-3: Similarly, the procedure is repeated for minimizing simultaneously loss and VSI in this case. The best objective function value 3.2352 is obtained by FSA via DGs at buses 56, 69, and 97 with sizes in kW, 342, 374 and 316, and CBs at buses 24, 48, and 77 with equal sizes of 150 kVAr. The minimum voltage magnitude 0.9956 p.u. is observed at 94th bus and correspondingly VSI is reached to 0.9826. In comparison to the base case, the real power losses (2.2526 kW) are decreased by 90.42%.

The comprehensive results of FSA for three cases under peak and average loading conditions are given in Table 2. The voltage profiles of the test system under different conditions are given in Fig. 2. For the results, it can be said that the P compensation via DGs has resulted in better results than only Q compensation via CBs and combined P and Q compensation has better results than either P or Q individual compensation.

The impact of CBs/DGs integration is resulted in minimizing the real power loss and grid dependency, consequently, GHG emission. As given in Eq. (12), the GHG emission before and after CBs/DGs integration is calculated for both peak and average loading conditions and presented

Fig. 1 The voltage profiles of 106-bus under peak loading conditions

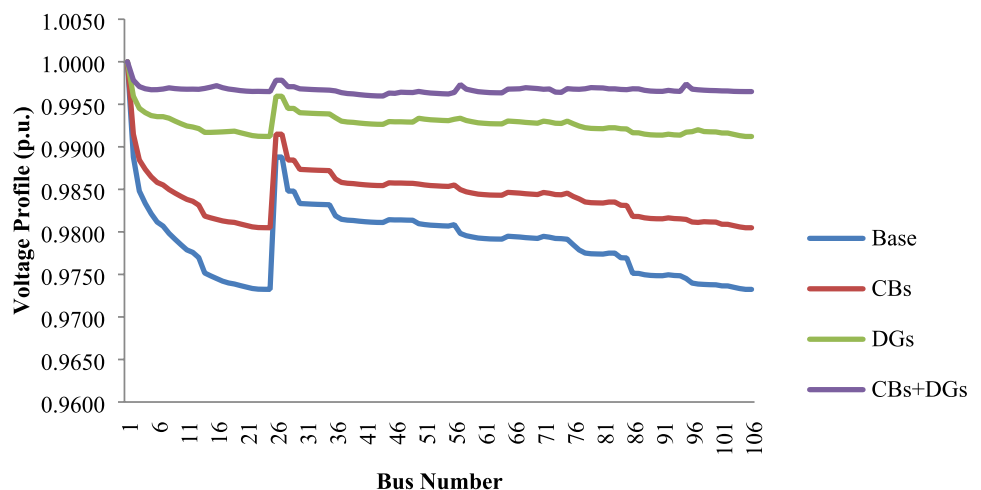
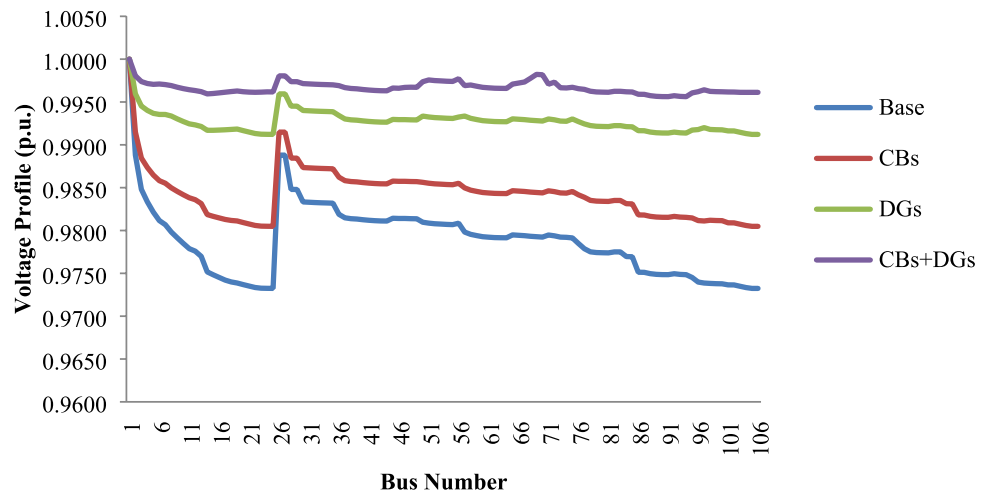


Table 2 FSA results of real-time 106-bus feeder under average loading conditions

Case	CBs (kVAr)	DGs (kW)	P_{loss} (kW)	Q_{loss} (kVAr)	V_{min} (p.u.)	VSI
Base	–	–	23.5169	17.1082	0.9732 (105)	0.8972
1	150 (8) 200 (98) 200 (77)	–	16.9252	12.3128	0.9805 (106)	0.9242
2	–	373 (97) 220 (7) 453 (8)	7.6946	5.5977	0.9912 (105)	0.9653
3	150 (24) 150 (48) 150 (77)	342 (56) 374 (69) 316 (97)	2.2526	1.6387	0.9956 (94)	0.9826

Fig. 2 The voltage profiles of 106-bus under average loading conditions

in Fig. 3. The percentage of reduction in GHG emission is calculated w.r.t. base case and given in Fig. 4. By observing Figs. 3 and 4, it can be said that the integration of CBs may result in improving system performance effectively but not in emission, since the grid dependency for total demand (load + loss) is not decreased much. On the other side, by having either DGs or combination of both DGs and CBs are results for reduced grid dependency and consequently the emission is decreased significantly and reduction rate is increased significantly. Notably, the emission reduction is more in Case-2 (i.e., only DGs) when compared with Case-3 (i.e., CBs and DGs), since the penetration of DGs is more in Case-2. Hence, at this point, it can be said that the integration of simultaneous allocation of CBs and DGs can contribute technically and environmentally in network operation.

5.2 Practical 36-bus residential feeder

The test system has 36 buses interconnecting by 35 branches, and serving a total constant power load of (2798.1 kW + j 1946.4 kVAr) at 11 kV. By considering 0.92 and 4.04 as exponents for real and reactive power in voltage-dependent load modeling for residential loads [26],

the load flow is performed. From the results, it is observed that total system load of (2791.1 kW + j 1922.9 kVAr) the test system is suffering from a total loss of (7.8571 kW + j 5.7163 kVAr). Also, the lowest voltage magnitude and stability index are observed as 0.9956 p.u. and 0.9825 at 11th bus respectively. Since it is a residential feeder, the performance improvement is simulated for only with DGs operating at upf (i.e., solar PV systems) for the following cases.

Case 1: Feeder performance improvement via optimal allocation of DGs with upf for base load considering loss minimization. The best DG sizes in kW are 789, 423 and 1193 at buses 6, 19 and 18 respectively. The real power compensation resulted as follows: In comparison, the real power loss decreased to 3.5736 kW and is equal to 54.52% reduction with base case. Correspondingly, the minimum voltage at the 11th bus is observed as 0.9974 p.u. and VSI is 0.9896.

Case 2: Analysis of feeder performance with EV loads penetration. At each bus, 10% load increment is assumed towards EVs adoption. In general EVs charge batteries via AC/DC charger and it is assumed that the operating power factor of the charger is 0.98, hence, the reactive power consumption by EV load is equal to 10% real power load $\times \tan(\cos^{-1}(0.98))$. As per voltage-dependent load modeling, the exponents of increased real and reactive

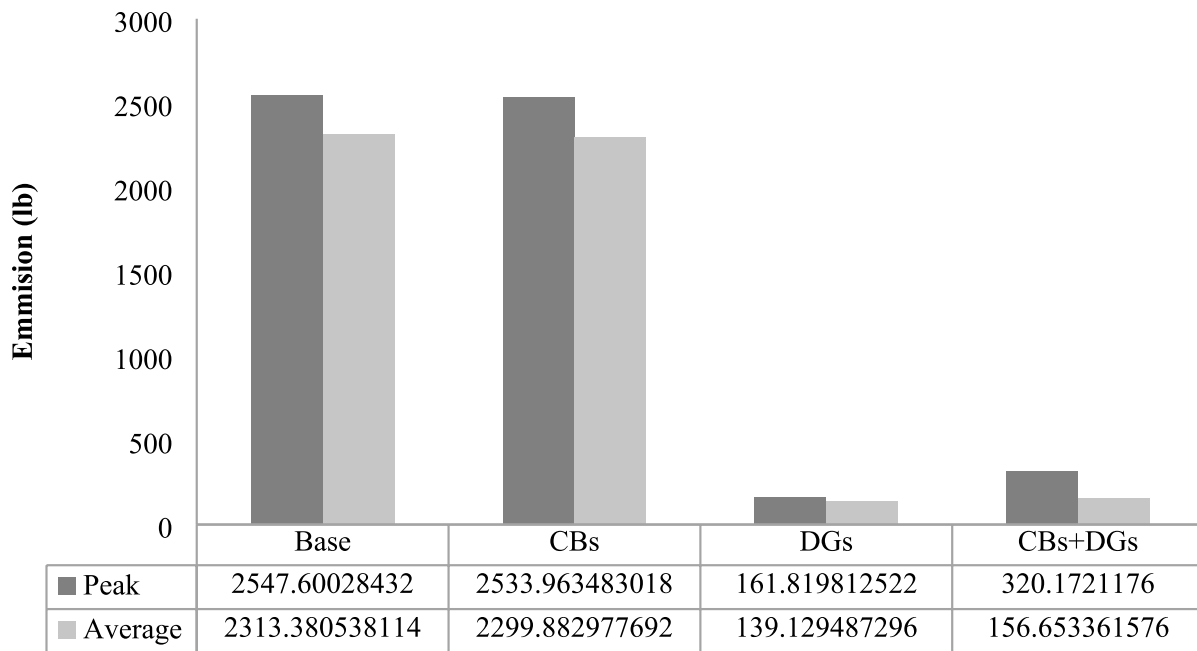
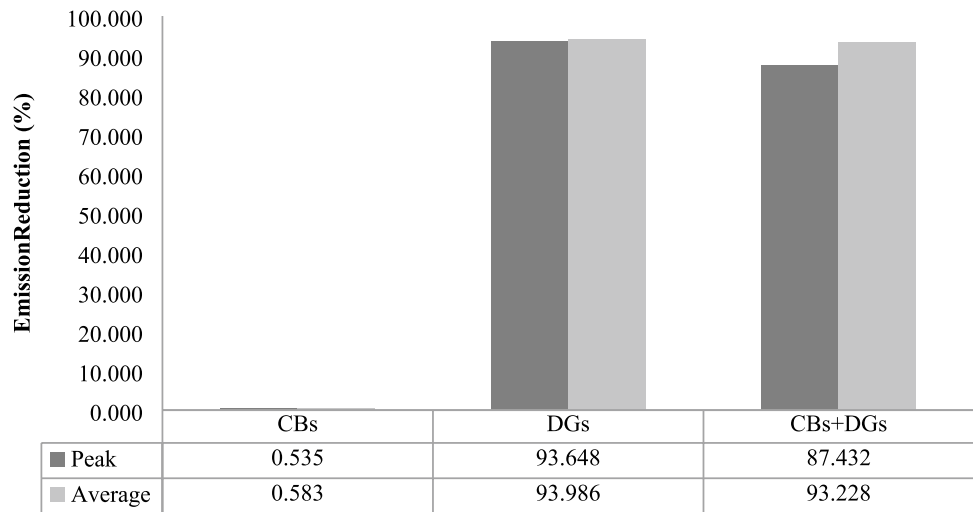


Fig. 3 GHG emission under different cases (106-bus system)

Fig. 4 Percentage of reduction in GHG emission under different cases (106-bus system)



power are considered as 2.59 and 4.06 respectively. The system load under this case is (3068.3 kW + j 1977.4 kVAr). Under these conditions, the system performance is as follows, the total losses are (9.0233 kW + j 6.5647 kVAr), lowest voltage at 11th bus is 0.9953 p.u. and correspondingly VSI is 0.9814. Here it can be observed that the losses are increased, voltage profile and VSI are decreased with additional EV load on the system.

Case 3: Feeder performance improvement via optimal allocation of DGs with upf considering loss minimization and VSI improvement: By using proposed FSA for solving DGs

allocation problem at this case, the best solution obtained is as follows: the locations of DGs are 36, 9 and 35 and their sizes in kW are 550, 541 and 1073 respectively. By having this real power compensation, the losses are decreased to (3.7216 kW + j 2.7075 kVAr), minimum voltage profile at 11th bus is increased to 0.9975 and VSI is raised to 0.99 respectively.

Case 4: Feeder performance improvement via optimal allocation of EV fleet considering loss minimization: In this case, the increased 10% of loading condition (279.11 kW + j 192.29 kVAr) across the network is taken as a load of

single EV fleet and optimized its location. The proposed FSA is finalized the 2nd bus as optimal location for EV fleet integration, correspondingly the system loading is (3069.74 kW + j 2114.45), the losses (8.1275 kW + j 5.9130), the lowest voltage at 11th bus is 0.9955 p.u and system stability index is 0.9823.

Case 5: Feeder performance improvement via simultaneous optimal allocation of DGs and EV fleet considering loss minimization and voltage stability maximization: In this case, the increased loading condition across the network is taken as total power rating of a single EV fleet and optimized its location along with DG locations and sizes. FSA resulted lowest objective function by EV fleet location at 2 and DGs sizes in kW and locations are: 1179(7), 1317(17), 427(30), correspondingly the losses (3.6418 kW + j 2.6495 kVar), lowest voltage at 11th bus is 0.9981 and VSI is 0.9923.

The comprehensive results of all the cases are given in Table 3 and correspondingly the voltage profiles are given in Fig. 5. From Fig. 3, the base case voltage profile across the network is improved by having DGs (case-1) declined. Similarly by having EV load distribution across the network, the voltage profile is declined significantly (case-2). At this stage also, it is also possible to improve network profile by having DGs at best locations (case-3). On the other side, by having a charging facility to support spatially distributed EV load (as seen in case-2) at some best locations as EV fleet, the voltage profile can be improved significantly (as seen in case -4). This situation can be further improved by having EV fleets and DGs at optimal locations (as seen in case-5). From these case studies, it can be said that the improved voltage profile is almost flat across the network in case-5, hence, the distribution losses are decreased and consequently VSI is improved significantly.

As determined in the 106-bus system, the GHG emission is calculated for different cases in this test system also and the percentage of reduction/increment in emission w.r.t. the base case is given in Fig. 6. In case-1, the grid dependency for base case loading is decreased via DGs allocation, whereas in case-2 and case-4, it is increased due to EV load. But as compared to case-2 (EV load is distributed spatially), in case-4, it is less due to concentrated EV load as fleet at optimal location. Hence, in case-2 and case-4,

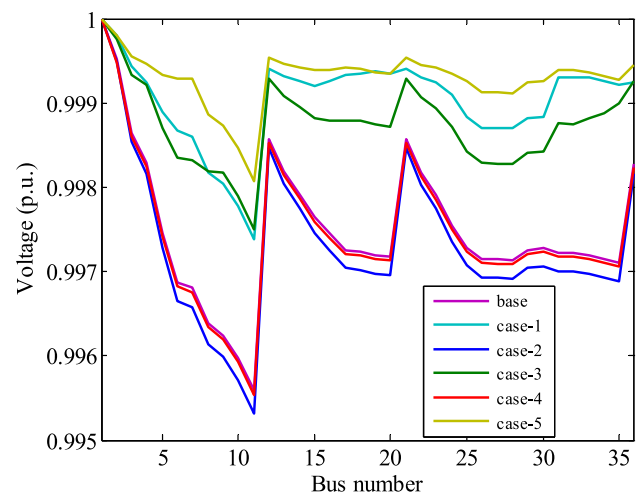


Fig. 5 Voltage profile 36-bus system for different cases

the emission is increased. The negative effect in case-2 and case-4 is managed effectively by having DGs in case-3 and case-5 respectively. Hence, in case-3 and case-5 resulted in reduction in emission. But as compared to case-3, case-5 is given more reduction in emission due to optimal location of both EV fleet and DGs in the network.

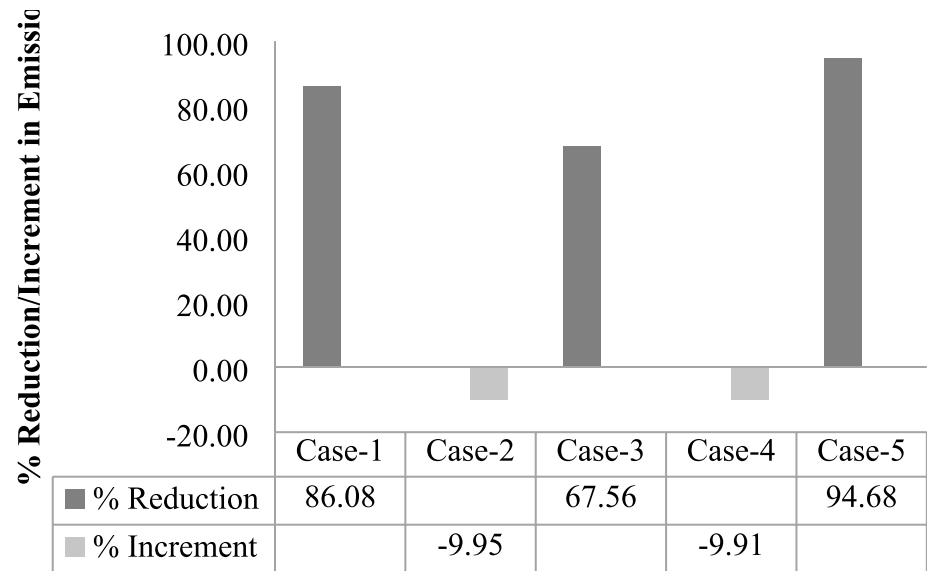
5.3 Comparison of FSA performance with other HSAs

The results of FSA for Case-5 are compared with other HAs, namely, Grasshopper Optimization Algorithm (GOA) [53], Teaching Learning-based Optimization (TLBO) [54], Cuckoo Search Algorithm (CSA) [55], Flower Pollination Algorithm (FPA) [56] and Particle Swarm Optimization (PSO) [57]. Since FSA is not required to control any parameters, we have not changed any parameters of other algorithms also. In PSO, the range for inertia weighting factor is decreased linearly about 0.9 to 0.4 during a run and the social and cognitive coefficients are taken equally as 2. In CSA, the switching parameter is set to 0.8. In TLBO, the teaching factor may become randomly either 1 or 2 with equal probability during a run. For GOA, the intensity of attraction and the scale of attractive length are considered as 0.5 and 1.5 respectively. For all algorithms, the following

Table 3 FSA results of real-time 36-bus feeder

Case	DGs (kW)	P _{loss} (kW)	Q _{loss} (kVar)	V _{min} (11) (p.u.)	VSI
Base	–	7.8571	5.7163	0.9956	0.9825
1	789 (6), 423 (19), 1193 (18)	3.5736	2.5999	0.9974	0.9896
2	–	9.0233	6.5647	0.9953	0.9814
3	550 (36), 541 (9), 1073 (35)	3.7216	2.7075	0.9975	0.99
4	–	8.1275	5.9130	0.9955	0.9823
5	1179(7), 1317(17), 427(30)	3.6418	2.6495	0.9981	0.9923

Fig. 6 Changes in emission reduction/increment w.r.t. EV load, fleet and DGs (36-bus system)



parameters are considered commonly: population = 50, iterations = 50, search variables = 7 (i.e., 3 for DG locations, 3 for DG sizes and 1 for EV fleet location). The lower limit and upper limits for locations = [2, nbus] and DG sizes = [0, 1500].

In order to determine the robustness of FSA in solving optimization problems, each algorithm is simulated for 25 independent run simulations for case-5 in the 36-bus system and compared their performance characteristics in terms of best, mean and worst objective functions. The boxplots given in Fig. 7 for Case 5 in the 36-bus system are allowed to clear and analyze these features. At this point, it can be said that the FSA is a more robust and efficient algorithm than other used algorithms. The best solution obtained by each algorithm over 25 independent run simulations are given along with average computational time in Table 4. Also, the best cost/solution improvement obtained by FSA is quantified and defined as [58]:

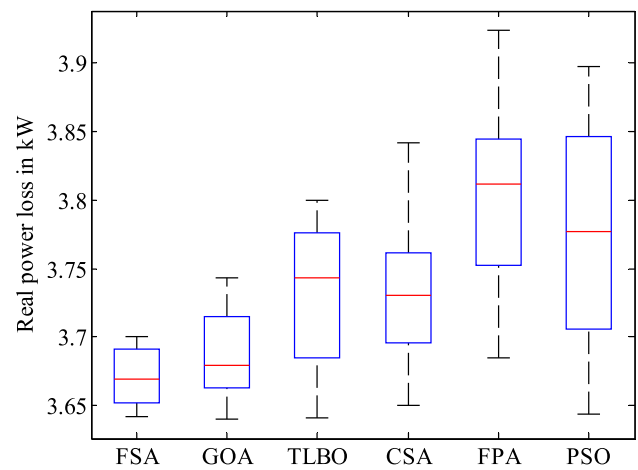


Fig. 7 Boxplot for comparison HSAs for case-5 in 36-bus system

$$BSI(\%) = \frac{\text{best solution of compared method} - \text{best solution of proposed FSA}}{\text{best solution of compared method}} \times 100\% \tag{23}$$

Table 4 Comparison of best solution obtained by different HSAs for case-5 (36-bus system)

Case	DGs sizes in kW and (bus)	Fleet Location	P_{loss} (kW)	Q_{loss} (kVAr)	V_{min} (11) (p.u.)	VSI	Time (s)	BSI (%)
PSO	1392 (33), 1127(8)	2	3.9111	2.8454	0.9985	0.9939	1.7301	6.8855
FPA	393(29), 966(7), 1376(33)	24	3.8949	2.8336	0.9976	0.9906	1.6537	6.4982
CSA	611(9), 526(17), 1442(23)	3	3.8760	2.8198	0.9976	0.9903	1.5425	6.0423
TLBO	1343(18), 1049(5), 374(13)	2	3.7569	2.7332	0.9973	0.9892	1.4139	3.0637
GOA	702(31), 888(5), 698(24)	2	3.7535	2.7307	0.9970	0.9881	1.3008	2.9759
FSA	1179(7), 1317(17), 427(30)	2	3.6418	2.6495	0.9981	0.9923	1.2581	NA

The more BSI value of an algorithm indicates more distance from the best solution obtained by proposed FSA. All these performance matrices are less with FSA over other compared algorithms, hence it can be said that the FSA is effective in resulting global solutions frequently. The convergence characteristics of different algorithms for case-5 in the 36-bus system for best solution provided in Table 4 are given as new Fig. 8.

6 Conclusion

This research presented the application of a new nature-inspired meta-heuristic algorithm called future search algorithm for solving the simultaneous allocation of distributed generation and electric vehicle fleets in radial distribution systems. The proposed methodology mimics human behavior in search for better living life by inspiring a local popular/ successful leader in a zone. In FSA, the population size indicates the number of nations searching by a person for his comfortable life. The more nations mean the more local influenced persons. These individual local best persons can again be influenced by a global best person. Hence defining new GS and LS at each iteration and again using them for updating the optimal solution within the same iteration is the key feature of FSA for out-performance over other HAs.

The simultaneous allocation of DGs and EVs has been formulated as a multi-objective function using real power loss, average voltage deviation index (AVDI), voltage stability index (VSI) and greenhouse gas (GHG) emission. In comparison with PSO, FPA, TLBO, CSA and GOA, the proposed FSA has resulted in the lowest objective function. The statistical analysis based on 25-individual run time

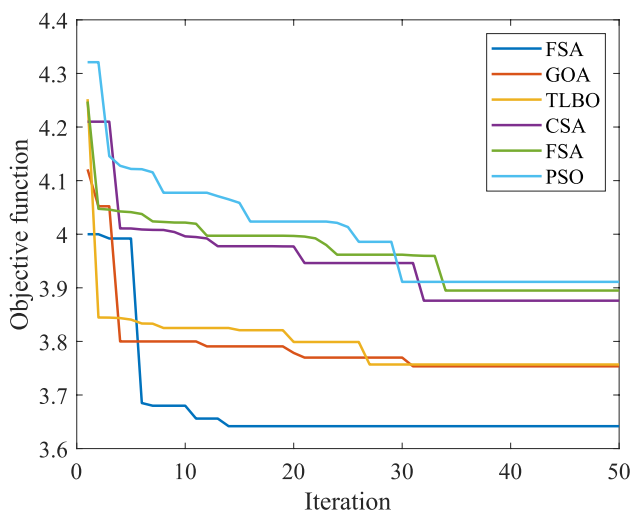


Fig. 8 Convergence characteristics of various algorithms

results, FSA has shown its superiority in terms of robustness and consistency. In conclusion, FSA has outperformed other simulated HAs in solving the multi-objective, non-linear and complex optimization problem.

The simulation results on a practical 106-bus agriculture feeder for simultaneous allocation of multiple DGs, and a 36-bus rural feeder for simultaneous allocation of DGs and EV fleet are presented. From the case studies, the EV load penetration has resulted in degrading the feeder performance significantly in terms of increased real power losses, decreased voltage profile and consequently resulted in lowering the voltage stability margin. In counter to this scenario, the optimal placement and sizing of DGs and EVs resulted for improvement in feeder performance significantly. Also, the environmental benefits in terms of reduced GHG emission have shown the necessity of the RE and EV technologies adoption globally.

However, the randomness in EV fleet load, intermittency of renewable energy and timely varying network loading conditions can create potential operating issues in the modern distribution networks. Under these circumstances, validation of proposed methodology for enhancing the performance of distribution network by using simultaneous smart charging scenario in EV fleets and timely optimal network reconfiguration w.r.t. network loading conditions need to be further analyzed. Also, the computational efficiency of the proposed meta-heuristic FSA algorithm in solving such complex multi-objective optimization problems needs to be further investigated and treated as future scope of this research.

Acknowledgement The authors wish to thank Mr. D. Venkata Chalpathi, SE, Operation, APSPDCL, Tirupati, Andhra Pradesh and Dr. N. M. G. Kumar, Professor, Dept of Electrical and Electronics Engineering, Sree Vidyanikethan Engineering College, Tirupati, Andhra Pradesh for providing the data of practical feeders used in this research.

Compliance with ethical standards

Conflict of interest The authors declare that they have no known competing financial interests or personal relationships that could have appeared to influence the work reported in this paper.

Open Access This article is licensed under a Creative Commons Attribution 4.0 International License, which permits use, sharing, adaptation, distribution and reproduction in any medium or format, as long as you give appropriate credit to the original author(s) and the source, provide a link to the Creative Commons licence, and indicate if changes were made. The images or other third party material in this article are included in the article's Creative Commons licence, unless indicated otherwise in a credit line to the material. If material is not included in the article's Creative Commons licence and your intended use is not permitted by statutory regulation or exceeds the permitted use, you will need to obtain permission directly from the copyright

holder. To view a copy of this licence, visit <http://creativecommons.org/licenses/by/4.0/>.

Appendix

A1: Practical 106-bus agriculture feeder data

Brach #	Fb #	Tb #	R (Ω)	X (Ω)	Average load at Tb		Peak load at Tb	
					Pd (kW)	Qd (kVAr)	Pd (kW)	Qd (kVAr)
1	1	2	0.8145	0.5925	0	0	0	0
2	2	3	0.2932	0.2133	0	0	0	0
3	3	4	0.1086	0.079	11.65	8.022	12.955	8.464
4	4	5	0.0977	0.0711	0	0	0	0
5	5	6	0.0977	0.0711	0	0	0	0
6	6	7	0.0543	0.0395	3.735	2.741	3.919	2.51
7	7	8	0.0977	0.0711	0	0	0	0
8	8	9	0.1086	0.079	11.88	7.784	12.944	8.138
9	9	10	0.1086	0.079	11.808	7.751	12.942	8.242
10	10	11	0.1086	0.079	11.966	7.717	12.94	8.01
11	11	12	0.0543	0.0395	10.512	9.409	11.944	9.842
12	12	13	0.1358	0.0988	3.636	2.693	3.903	2.651
13	13	14	0.4344	0.316	3.956	1.78	3.895	2.146
14	14	15	0.1086	0.079	18.428	11.748	19.895	12.91
15	15	16	0.1086	0.079	0	0	0	0
16	16	17	0.1086	0.079	18.54	11.69	20.887	12.748
17	17	18	0.0815	0.0593	11.578	8.34	12.929	8.563
18	18	19	0.0543	0.0395	11.664	7.497	12.929	8.445
19	19	20	0.1086	0.079	11.621	7.487	12.928	8.504
20	20	21	0.1358	0.0988	0	0	0	0
21	21	22	0.1629	0.1185	12.038	7.469	12.927	7.902
22	22	23	0.1086	0.079	0	0	0	0
23	23	24	0.0543	0.0395	11.966	7.464	12.927	8.01
24	24	25	0.0543	0.0395	11.534	8.294	12.927	8.621
25	2	26	0.0652	0.0474	3.623	2.848	3.953	2.67
26	26	27	0.0326	0.0237	3.78	2.848	3.953	2.442
27	3	28	0.0543	0.0395	11.923	8.1	12.959	8.074
28	28	29	0.0543	0.0395	3.74	2.795	3.936	2.503
29	4	30	0.0543	0.0395	12.038	8.022	12.955	7.902
30	4	31	0.0543	0.0395	11.923	8.017	12.955	8.074
31	31	32	0.0543	0.0395	11.966	8.017	12.955	8.01
32	32	33	0.0543	0.0395	12.053	8.012	12.955	7.88
33	33	34	0.0543	0.0395	12.038	8.012	12.955	7.902
34	34	35	0.1086	0.079	18.473	12.463	20.927	12.846
35	5	36	0.1086	0.079	18.833	12.349	20.921	12.312
36	36	37	0.1955	0.1422	0	0	0	0
37	37	38	0.1086	0.079	11.651	7.909	12.95	8.462

Brach #	Fb #	Tb #	R (Ω)	X (Ω)	Average load at Tb		Peak load at Tb	
					Pd (kW)	Qd (kVAr)	Pd (kW)	Qd (kVAr)
38	38	39	0.0543	0.0395	3.654	2.75	3.922	2.626
39	39	40	0.1086	0.079	12.038	7.904	12.949	7.902
40	40	41	0.1086	0.079	11.822	7.9	12.949	8.221
41	41	42	0.1086	0.079	11.923	7.9	12.949	8.074
42	42	43	0.1086	0.079	11.966	7.895	12.949	8.01
43	43	44	0.0543	0.0395	11.938	7.895	12.949	8.053
44	37	45	0.1086	0.079	18.473	12.311	20.919	12.846
45	45	46	0.1195	0.0869	18.495	12.311	20.919	12.813
46	37	47	0.1086	0.079	18.833	12.311	20.919	12.312
47	47	48	0.0543	0.0395	18.698	12.303	20.919	12.516
48	48	49	0.0543	0.0395	18.135	13.182	19.923	13.318
49	6	50	0.1629	0.1185	18.923	12.266	20.917	12.173
50	50	51	0.1086	0.079	12.398	7.005	13.944	7.324
51	51	52	0.1086	0.079	11.693	7.875	12.948	8.405
52	52	53	0.0706	0.0514	11.592	7.875	12.948	8.543
53	53	54	0.1086	0.079	11.851	7.875	12.948	8.18
54	54	55	0.1086	0.079	19.17	11.369	20.916	11.78
55	51	56	0.0543	0.0395	12.11	7.88	12.948	7.791
56	8	57	0.1086	0.079	3.74	2.73	3.915	2.503
57	8	58	0.1086	0.079	0	0	0	0
58	58	59	0.1086	0.079	11.707	7.798	12.944	8.385
59	59	60	0.1086	0.079	11.592	7.794	12.944	8.543
60	60	61	0.0977	0.0711	12.197	7.789	13.939	7.655
61	61	62	0.1086	0.079	11.621	7.789	12.944	8.504
62	62	63	0.0543	0.0395	11.894	7.789	12.944	8.117
63	63	64	0.0543	0.0395	11.635	7.789	12.944	8.484
64	58	65	0.0543	0.0395	11.966	7.803	12.944	8.01
65	65	66	0.0543	0.0395	3.789	2.725	3.913	2.428
66	66	67	0.0543	0.0395	18.293	12.997	19.914	13.101
67	67	68	0.1629	0.1185	11.549	8.665	12.944	8.601
68	68	69	0.1629	0.1185	11.563	8.66	12.944	8.582
69	69	70	0.3258	0.237	11.65	7.789	12.944	8.464
70	65	71	0.0977	0.0711	11.664	7.803	12.944	8.445
71	67	72	0.1358	0.0988	11.693	7.798	12.944	8.405
72	60	73	0.1086	0.079	18.248	12.981	19.913	13.164
73	73	74	0.1086	0.079	18.473	12.116	20.909	12.846
74	9	75	0.0543	0.0395	11.606	7.784	12.944	8.524
75	10	76	0.0543	0.0395	11.707	7.751	12.942	8.385
76	11	77	0.0543	0.0395	11.866	7.717	12.94	8.159
77	12	78	0.1086	0.079	0	0	0	0
78	78	79	0.1901	0.1383	11.693	7.694	12.939	8.405
79	79	80	0.0815	0.0593	11.765	7.689	12.939	8.304
80	80	81	0.1086	0.079	11.722	7.689	12.939	8.364
81	78	82	0.0543	0.0395	11.491	8.548	12.939	8.678
82	78	83	0.0543	0.0395	11.794	7.694	12.939	8.263
83	13	84	0.0543	0.0395	11.477	8.517	12.938	8.697
84	84	85	0.1629	0.1185	11.966	7.665	12.938	8.01
85	14	86	0.1086	0.079	18.225	12.611	19.896	13.195

Brach #	Fb	Tb	R (Ω)	X (Ω)	Average load at Tb		Peak load at Tb	
					Pd (kW)	Qd (kVAr)	Pd (kW)	Qd (kVAr)
					86	86	87	0.0815
87	14	88	0.3258	0.237	0	0	0	0
88	88	89	0.1629	0.1185	11.578	8.392	12.932	8.563
89	89	90	0.1629	0.1185	0	0	0	0
90	90	91	0.1086	0.079	3.618	2.666	3.894	2.676
91	88	92	0.0543	0.0395	11.765	7.557	12.932	8.304
92	89	93	0.0543	0.0395	11.52	8.392	12.932	8.64
93	90	94	0.0543	0.0395	11.506	8.392	12.932	8.659
94	16	95	0.0543	0.0395	3.654	2.661	3.892	2.626
95	18	96	0.1086	0.079	11.722	7.506	12.929	8.364
96	19	97	0.0543	0.0395	3.65	2.653	3.889	2.633
97	19	98	0.1086	0.079	11.693	7.497	12.929	8.405
98	98	99	0.1086	0.079	11.549	8.325	12.929	8.601
99	99	100	0.1086	0.079	11.635	7.492	12.929	8.484
100	20	101	0.1086	0.079	11.563	8.319	12.928	8.582
101	101	102	0.0543	0.0395	11.851	7.487	12.928	8.18
102	21	103	0.1086	0.079	18.27	12.464	19.889	13.132
103	22	104	0.0543	0.0395	11.707	7.469	12.927	8.385
104	23	105	0.1086	0.079	18.225	12.441	19.888	13.195
105	23	106	0.1086	0.079	18.36	11.611	19.888	13.006

A2: Practical 36-bus residential feeder data

Brach #	Fb	Tb	R (Ω)	X (Ω)	Load at Tb	
					Pd (kW)	Qd (kVAr)
1	1	2	0.01358	0.00988	65.406	75.644
2	2	3	0.02606	0.01896	97.800	20.861
3	3	4	0.02715	0.01975	100.000	0.000
4	4	5	0.07222	0.05254	88.200	47.125
5	5	6	0.05702	0.04148	90.566	42.401
6	6	7	0.00652	0.00474	175.928	261.294
7	7	8	0.06570	0.04780	98.410	17.762
8	8	9	0.02552	0.01857	210.300	135.181
9	9	10	0.08688	0.06320	56.007	28.848
10	10	11	0.16833	0.12245	61.740	308.890
11	3	12	0.00380	0.00277	0.000	0.000
12	12	13	0.02172	0.01580	0.000	0.000
13	13	14	0.01629	0.01185	0.000	0.000
14	14	15	0.01629	0.01185	0.000	0.000
15	15	16	0.01846	0.01343	76.000	64.992
16	16	17	0.02063	0.01501	0.000	0.000
17	17	18	0.00217	0.00158	0.000	0.000
18	18	19	0.01955	0.01422	86.000	134.922
19	19	20	0.03149	0.02291	51.975	35.603
20	12	21	0.00326	0.00237	118.400	107.617
21	13	22	0.01629	0.01185	98.500	17.255

Brach #	Fb	Tb	R (Ω)	X (Ω)	Load at Tb	
					Pd (kW)	Qd (kVAr)
22	14	23	0.00652	0.00474	62.559	7.441
23	15	24	0.01629	0.01185	100.000	0.000
24	24	25	0.05159	0.03753	55.900	82.917
25	25	26	0.06136	0.04464	26.560	96.408
26	26	27	0.00163	0.00119	99.732	7.316
27	27	28	0.00977	0.00711	19.996	59.742
28	25	29	0.02172	0.01580	86.000	51.029
29	25	30	0.00163	0.00119	88.180	47.162
30	17	31	0.01629	0.01185	98.825	15.285
31	31	32	0.00380	0.00277	100.000	0.000
32	18	33	0.00760	0.00553	88.500	46.559
33	33	34	0.01086	0.00790	183.600	79.316
34	34	35	0.01629	0.01185	219.200	120.214
35	4	36	0.00815	0.00593	93.800	34.664

References

- Rissman J et al (2020) Technologies and policies to decarbonize global industry: review and assessment of mitigation drivers through 2070. *Appl Energy* 266:114848. <https://doi.org/10.1016/j.apenergy.2020.114848>
- Renewable capacity statistics 2019 (2019) International Renewable Energy Agency. ISBN: 978-92-9260-123-2. <https://www.irena.org/publications/2019/Mar/Renewable-Capacity-Statistics-2019>
- Global EV Outlook (2019) International Energy Agency. <https://www.iea.org/reports/global-ev-outlook-2019>
- Ha MP, Huy PD, Ramachandaramurthy VK (2017) A review of the optimal allocation of distributed generation: objectives, constraints, methods, and algorithms. *Renew Sustain Energy Rev* 75:293–312. <https://doi.org/10.1016/j.rser.2016.10.071>
- Ehsan A, Yang Q (2018) Optimal integration and planning of renewable distributed generation in the power distribution networks: a review of analytical techniques. *Appl Energy* 210:44–59. <https://doi.org/10.1016/j.apenergy.2017.10.106>
- Nguyen TP, Tran TT, Vo DN (2019) Improved stochastic fractal search algorithm with chaos for optimal determination of location, size, and quantity of distributed generators in distribution systems. *Neural Comput Appl* 31:7707–7732. <https://doi.org/10.1007/s00521-018-3603-1>
- Dehghani M, Montazeri Z, Malik OP (2020) Optimal sizing and placement of capacitor banks and distributed generation in distribution systems using spring search algorithm. *Int J Emerg Electr Power Syst*. <https://doi.org/10.1515/ijeeeps-2019-0217>
- Dixit M, Kundu P, Jariwala HR (2017) Incorporation of distributed generation and shunt capacitor in Radial distribution network for techno-economic benefits. *Eng Sci Technol Int J* 20(2):482–493. <https://doi.org/10.1016/j.jestch.2017.01.003>
- Mohanty B, Tripathy S (2016) A teaching learning based optimization technique for optimal location and size of DG in distribution network. *J Electr Syst Inf Technol* 3(1):33–44. <https://doi.org/10.1016/j.jesit.2015.11.007>
- Kowsalya MIA (2014) Optimal distributed generation and capacitor placement in power distribution networks for power loss minimization. In: Proceedings of international conference on

- advanced electrical engineering (ICAEE). pp 1–6. <https://doi.org/10.1109/ICAEE.2014.6838519>
11. Sanjay R et al (2017) Optimal allocation of distributed generation using hybrid grey wolf optimizer. *IEEE Access* 5:14807–14818. <https://doi.org/10.1109/ACCESS.2017.2726586>
 12. Mahmoud K, Lehtonen M (2019) Simultaneous allocation of multi-type distributed generations and capacitors using generic analytical expressions. *IEEE Access* 7:182701–182710. <https://doi.org/10.1109/ACCESS.2019.2960152>
 13. Almabsout EA et al (2020) A hybrid local Search-Genetic algorithm for simultaneous placement of DG units and shunt capacitors in Radial distribution networks. *IEEE Access* 8:54465–54481. <https://doi.org/10.1109/ACCESS.2020.2981406>
 14. Coelho FCR, da-Silva IC Jr, Dias BH et al (2018) Optimal distributed generation allocation using a new metaheuristic. *J Control Autom Electr Syst* 29:91–98. <https://doi.org/10.1007/s40313-017-0346-7>
 15. Rajeswaran S, Nagappan K (2016) Optimum simultaneous allocation of renewable energy DG and capacitor banks in radial distribution network. *Circ. Syst.* 7(11):3556–3564. <https://doi.org/10.4236/cs.2016.711302>
 16. Ali ES, Abd-Elazim SM, Abdelaziz AY (2018) Optimal allocation and sizing of renewable distributed generation using ant lion optimization algorithm. *Electr Eng* 100(1):99–109. <https://doi.org/10.1007/s00202-016-0477-z>
 17. Elsayed AM, Mishref MM, Farrag SM (2019) Optimal allocation and control of fixed and switched capacitor banks on distribution systems using grasshopper optimisation algorithm with power loss sensitivity and rough set theory. *IET Gener Transm Distrib.* <https://doi.org/10.1049/iet-gtd.2018.5494>
 18. Kansal S, Tyagi B, Kumar V (2017) Cost–benefit analysis for optimal distributed generation placement in distribution systems. *Int J Ambient Energy* 38(1):45–54. <https://doi.org/10.1080/01430750.2015.1031407>
 19. Suresh MCV, Belwin Edward J (2017) Optimal placement of distributed generation in distribution systems by using shuffled frog leaping algorithm. *ARPN J Eng Appl Sci* 12(3):863–868
 20. Alilou M, Farsadi M, Shayeghi H (2018) Optimal allocation of renewable DG and capacitor for improving technical and economic indices in real distribution system with nonlinear load model. *J Energy Manag Technol* 2(4):18–28. <https://doi.org/10.22109/JEMT.2018.122495.1071>
 21. Sambaiah KS, Jayabarathi T (2019) Optimal allocation of renewable distributed generation and capacitor banks in distribution systems using Salp Swarm algorithm. *Int J Renew Energy Res* 9:96–107
 22. Abou El-Ela AA, El-Sehiemy RA, Abbas AS (2018) Optimal placement and sizing of distributed generation and capacitor banks in distribution systems using water cycle algorithm. *IEEE Syst J* 12(4):3629–3636. <https://doi.org/10.1109/JSYST.2018.2796847>
 23. Suresh MCV, Edward JB (2020) A hybrid algorithm based optimal placement of DG units for loss reduction in the distribution system. *Appl Soft Comput.* <https://doi.org/10.1016/j.asoc.2020.106191>
 24. Samala RK, Kotapuri MR (2020) Optimal allocation of distributed generations using hybrid technique with fuzzy logic controller radial distribution system. *SN Appl Sci* 2:191. <https://doi.org/10.1007/s42452-020-1957-3>
 25. Vijay R (2018) Optimal allocation of electric power distributed generation on distributed network using elephant herding optimization technique. *CVR J Sci Technol* 15:73–79. <https://doi.org/10.32377/cvrjst1513>
 26. Hadidian-Moghaddam MJ et al (2018) A multi-objective optimal sizing and siting of distributed generation using ant lion optimization technique. *Ain Shams Eng J* 9(4):2101–2109. <https://doi.org/10.1016/j.asej.2017.03.001>
 27. Kumar M, Nallagownden P, Elamvazuthi I (2017) Optimal placement and sizing of renewable distributed generations and capacitor banks into Radial distribution networks. *Energies* 10(6):811. <https://doi.org/10.3390/en10060811>
 28. Truong KH, Nallagownden P, Elamvazuthi I, Vo DN (2020) A quasi-oppositional-chaotic symbiotic organisms search algorithm for optimal allocation of DG in radial distribution networks. *Appl Soft Comput* 88:106067. <https://doi.org/10.1016/j.asoc.2020.106067>
 29. Truong KH, Nallagownden P, Elamvazuthi I et al (2020) An improved meta-heuristic method to maximize the penetration of distributed generation in radial distribution networks. *Neural Comput Appl* 32:10159–10181. <https://doi.org/10.1007/s00521-019-04548-4>
 30. Nguyen TT, Nguyen TT, Nguyen NA, Duong TL (2020) A novel method based on coyote algorithm for simultaneous network reconfiguration and distribution generation placement. *Ain Shams Eng J.* <https://doi.org/10.1016/j.asej.2020.06.005>
 31. Pham TD, Nguyen TT, Dinh BH (2020) Find optimal capacity and location of distributed generation units in radial distribution networks by using enhanced coyote optimization algorithm. *Neural Comput Appl.* <https://doi.org/10.1007/s00521-020-05239-1>
 32. Roosta A, Eskandari HR, Khooban MH (2019) Optimization of radial unbalanced distribution networks in the presence of distribution generation units by network reconfiguration using harmony search algorithm. *Neural Comput Appl* 31:7095–7109. <https://doi.org/10.1007/s00521-018-3507-0>
 33. Selim A, Kamel S, Jurado F (2020) Efficient optimization technique for multiple DG allocation in distribution networks. *Appl Soft Comput* 86:105938. <https://doi.org/10.1016/j.asoc.2019.105938>
 34. Nagaballi S, Kale VS (2020) Pareto optimality and game theory approach for optimal deployment of DG in radial distribution system to improve techno-economic benefits. *Appl Soft Comput* 92:106234. <https://doi.org/10.1016/j.asoc.2020.106234>
 35. Nguyen TT, Nguyen TT, Duong LT et al (2020) An effective method to solve the problem of electric distribution network reconfiguration considering distributed generations for energy loss reduction. *Neural Comput Appl.* <https://doi.org/10.1007/s00521-020-05092-2>
 36. Ha MP, Nazari-Heris M, Mohammadi-Ivatloo B, Seyedi H (2020) A hybrid genetic particle swarm optimization for distributed generation allocation in power distribution networks. *Energy* 209:118218. <https://doi.org/10.1016/j.energy.2020.118218>
 37. Nguyen TT, Dinh BH, Pham TD, Nguyen TT (2020) Active power loss reduction for radial distribution systems by placing capacitors and PV systems with geography location constraints. *Sustainability* 12(18):7806. <https://doi.org/10.3390/su12187806>
 38. Duong MQ, Pham TD, Nguyen TT, Doan AT, Tran HV (2019) Determination of optimal location and sizing of solar photovoltaic distribution generation units in radial distribution systems. *Energies* 12(1):174. <https://doi.org/10.3390/en12010174>
 39. Resener M et al (2018) Optimization techniques applied to planning of electric power distribution systems: a bibliographic survey. *Energy Syst* 9(3):473–509. <https://doi.org/10.1007/s12667-018-0276-x>
 40. Kalambe S, Agnihotri G (2014) Loss minimization techniques used in distribution network: bibliographical survey. *Renew Sustain Energy Rev* 29:184–200. <https://doi.org/10.1016/j.rser.2013.08.075>
 41. Sultana U et al (2016) A review of optimum DG placement based on minimization of power losses and voltage stability enhancement of distribution system. *Renew Sustain Energy Rev* 63:363–378. <https://doi.org/10.1016/j.rser.2016.05.056>

42. Badran O et al (2017) Optimal reconfiguration of distribution system connected with distributed generations: a review of different methodologies. *Renew Sustain Energy Rev* 73:854–867. <https://doi.org/10.1016/j.rser.2017.02.010>
43. Galadima AA, Zarma TA, Aminu MA (2019) Review on optimal siting of electric vehicle charging infrastructure. *J Sci Res Rep* 25(1):1–10 (**Article no.JSRR.50681**)
44. Wolpert DH, Macready WG (1997) No free lunch theorems for optimization. *IEEE Trans Evol Comput* 1(1):67–82. <https://doi.org/10.1109/4235.585893>
45. Elsis M (2019) Future search algorithm for optimization. *Evol Intell* 12:21–31. <https://doi.org/10.1007/s12065-018-0172-2>
46. Kongjeen Y, Bhumkittipich K (2018) Impact of plug-in electric vehicles integrated into power distribution system based on voltage-dependent power flow analysis. *Energies* 11(6):1571. <https://doi.org/10.3390/en11061571>
47. Hajagos LM, Danai B (1998) Laboratory measurements and models of modern loads and their effect on voltage stability studies. *IEEE Trans Power Syst* 13:584–592. <https://doi.org/10.1109/59.667386>
48. Wu Y-K, Chang SM, Hu Y-L (2017) Literature review of power system blackouts. *Energy Procedia* 141:428–431. <https://doi.org/10.1016/j.egypro.2017.11.055>
49. Sadeghi SE, Foroud AA (2019) A new approach for static voltage stability assessment in distribution networks. *Int Trans Electr Energy Syst*. <https://doi.org/10.1002/2050-7038.12203>
50. El-Ela AAA, El-Sehiemy RA, Abbas AS (2018) Optimal placement and sizing of distributed generation and capacitor banks in distribution systems using water cycle algorithm. *IEEE Syst J* 12(4):3629–3636. <https://doi.org/10.1109/JSYST.2018.2796847>
51. Elsis M (2021) Future search algorithm for optimization (<https://www.mathworks.com/matlabcentral/fileexchange/74027-future-search-algorithm-for-optimization>), MATLAB Central File Exchange. Retrieved January 27, 2021.
52. Satyanarayana S, Ramana T, Sivanagaraju S, Rao GK (2007) An efficient load flow solution for radial distribution network including voltage dependent load models. *Electr Power Compon Syst* 35(5):539–551. <https://doi.org/10.1080/15325000601078179>
53. Topaz CM, Bernoff AJ, Logan S, Toolson W (2008) A model for rolling swarms of locusts. *Eur Phys J Spec Top* 157:93–109. <https://doi.org/10.1140/epjst/e2008-00633-y>
54. Rao RV, Savsani VJ, Vakharia DP (2011) Teaching–learning-based optimization: a novel method for constrained mechanical design optimization problems. *Comput Aided Des* 43(3):303–315. <https://doi.org/10.1016/j.cad.2010.12.015>
55. Yang X-S, Deb S (2009) Cuckoo search via Lévy flights. In: Proceedings of world congress on nature and biologically inspired computing. IEEE Publications, USA, pp 210–214. <https://doi.org/10.1109/NABIC.2009.5393690>
56. Yang X-S (2012) Flower pollination algorithm for global optimization. In: International conference on unconventional computing and natural computation. Springer, Berlin, Heidelberg. https://doi.org/10.1007/978-3-642-32894-7_27
57. Kennedy J, Eberhart RC (1995) Particle swarm optimization. In: Proceedings of IEEE International Conference on Neural Networks, Perth, Australia, vol 4. pp 1942–1948. <https://doi.org/10.1109/ICNN.1995.488968>
58. Nguyen TT, Quynh NV, Dai LV (2018) Improved firefly algorithm: a novel method for optimal operation of thermal generating units. *Complexity* 2018:23. <https://doi.org/10.1155/2018/7267593>

Publisher's Note Springer Nature remains neutral with regard to jurisdictional claims in published maps and institutional affiliations.